Nanoscale

Electrical conductivity of a single parallel contact between carbon nanotubes

Journal:	*Nanoscale*
Manuscript ID	NR-COM-07-2022-004112
Article Type:	Communication
Date Submitted by the Author:	26-Jul-2022
Complete List of Authors:	Hamasaki, Hiromu; Osaka University, Nagahama, Sougo; Osaka University Hirahara, Kaori; Osaka University, Center for Atomic and Molecular Technologies

COMMUNICATION

Electrical conductivity of a single parallel contact between carbon nanotubes

Received 00th January 20xx,
Accepted 00th January 20xx

DOI: 10.1039/x0xx00000x

Hiromu Hamasaki,*[a] Sougo Nagahama [a] and Kaori Hirahara [b]

Interfacial resistance plays a critical role in the transport properties of nanomaterial-based assemblies. However, understanding of them remains limited due to the difficulty of experimental approaches. Here we report *in situ* measurements of the electrical resistance of a single parallel contact between carbon nanotubes. By varying the contact length systematically, we derive the electrical conductivities of carbon nanotubes and interfaces. The interface between nanotubes exhibits conductivity intermediate between those of pyrolytic and single-crystal graphite. The threshold contact length between interface- and bulk-dominant electrical transport is quantitatively estimated.

Introduction

Carbon nanotubes (CNTs) have drawn considerable attention due to their superior thermal and electrical transport properties, in addition to the unique structure, outstanding mechanical strength, low density, and flexibility. The combination of these properties can provide broad potential applications such as lightweight conductors [1,2], biological sensors [3,4], and flexible thermoelectric generators [5,6]. Experimentally measured thermal and electrical conductivities for individual multiwalled carbon nanotubes (MWCNTs) are typically 10^3 W/m K [7,8] and 10^5 S/m [9,10], respectively. However, it is well known that in CNT assemblies, the conductivities are reduced by several orders of magnitude and depend on the alignment of individual nanotube axes. For example, Inoue *et al*. reported the thermal and electrical conductivities of a sheet of aligned MWCNTs as follows: 70 W/m K and 4×10^4 S/m along the direction parallel to the nanotube axial direction, but 8.6 W/m K and 5.5×10^3 S/m along the perpendicular direction [11]. Even for a bundle consisting of close-packed CNTs, decrements in conductivity [7,12] and conductivity anisotropy [13] have been experimentally detected. These findings indicate that the conductivity reductions cannot be solely attributed to the spacing within assemblies and that the difference between intratube and intertube bondings in assemblies is rather important. Probably due to the difficulty of the relevant experimental approaches, less is known about transport via a single contact between two neighboring nanotubes than about transport within an isolated nanotube, despite their likely equivalent importance for CNT assembly applications. To date, several experimental studies have examined the contact thermal [14] and electrical resistances [15–17] of a single contact between CNTs, and their findings have mainly focused on the point contacts between two nonparallel CNTs where the contact morphologies are nontrivial. To deepen the understanding of contact transport, systematic studies of the effects of contact length (or area) in simple, parallelly contacted CNTs would be of great importance. In addition, the methodology can be applied to a contact between other nanowires [18,19] and a hetero-contact in composites [20,21]. In this study, we experimentally investigate the electrical resistance of a single parallel contact between two MWCNTs. A nanomanipulation system equipped in a transmission electron microscope (TEM) enables the performance of *in situ* measurements of electrical resistance for a range of contact lengths.

Results and discussion

MWCNTs produced by the arc discharge method (412988, Sigma–Aldrich) were set on the edge of a platinum-coated silicon substrate. Subsequently, tin (Sn) particles were deposited by vacuum vapor deposition on the substrate to affix the MWCNTs to the substrate. A MWCNT protruding from the edge of the substrate was brought into contact with a Sn-coated cantilevered probe tip in TEM by controlling the manipulator [Figure 1 (a) and (b)]. The acceleration voltage of TEM was set for 90 kV to avoid the radiation damage. By applying voltage

[a] Department of Mechanical Engineering, Osaka University, 2-1 Yamadaoka, Suita, Osaka, 565-0871, Japan.
[b] Department of Mechanical Engineering and Center for Atomic and Molecular Technologies, Osaka University, 2-1 Yamadaoka, Suita, Osaka, 565-0871, Japan.
† Electronic Supplementary Information (ESI) available. See DOI: 10.1039/x0xx00000x

between the substrate and cantilevered tip, the bridged MWCNT was Joule-heated, particularly at the contact point between the end portion of the MWCNT and probe tip due to the high contact resistance. Since Sn particles existing beneath such a hot spot on the tip (and on MWCNT) melted, the MWCNT was welded onto the probe tip with good electrical and physical contact. Further Joule heating with increasing current cut the MWCNT off near the bridging center, and the contaminations evaporated along with most of the Sn particles decorating the surface [Fig. 1 (c)]. By this method, a pair of parallel, contamination-free MWCNTs were obtained. The MWCNTs were approached each other by operating the manipulator, then the contact was spontaneously formed by van der Waals force [Fig. 1(d)]. Electrical resistance measurements of the parallel-contacted MWCNTs were then carried out by applying a sweep current in the range of −1 to 1 μA so as to avoid changes in temperature due to self-Joule heating. It was verified that the measured resistance was independent of the exposure dose in TEM. The contact length was varied by translating one of the MWCNTs parallel to its axis [Fig. 1(d)–(f)]. Figure 1(g) presents three current–voltage relationships obtained from the parallel-contacted MWCNTs at contact lengths of 177, 69, and 35 nm, which correspond to the images shown in Fig. 1(d), (e), and (f), respectively. The relationships are almost linear with constant resistance in this measurement range, and resistance increases with decreasing the contact length.

Figure 2 presents the results of electrical resistance measurements for various contact lengths for pairs of parallel-contacted MWCNTs. The legend in the graph denotes the outer diameter of each MWCNT. The number of walls typically ranged from 10 to 20. Results at all contact lengths show the same trend; electrical resistance decreases with the increase of the contact length. This is qualitatively reasonable because the contact area increases in proportion to the contact length. Notably, we cannot directly attribute the measured resistance values to the contact resistance between CNTs, since they were obtained by the so-called two-terminal method. The total resistance R_{total} can be divided into three elements, namely,

$$R_{\mathrm{total}} = R_{\mathrm{CNT}} + R_{\mathrm{inter}} + R_0, \#(1)$$

where R_{CNT}, R_{inter}, and R_0 represent the resistance of the individual MWCNTs, the interfacial resistance between MWCNTs and other resistance, respectively. R_0 is generally non-zero in two-terminal method but can be assumed to be a constant value, as it is originated in components independent of the nature of CNTs and the contact between CNTs. The contact-length-dependent behaviour shown in Fig. 2 can be derived from the first two terms, R_{CNT} and R_{inter}. Here, the interfacial resistance R_{inter} can be represented as

$$R_{\mathrm{inter}} = \rho_{\mathrm{inter}}\frac{l}{A} = \rho_{\mathrm{inter}}\frac{l}{Cx} = \frac{\alpha}{x}, \#(2)$$

where ρ_{inter} represents the electrical resistivity of the interface, while l and A represent the length and cross-sectional area that contribute to contact transport, respectively. Since the cross-sectional area A is proportional to the contact length x, the interfacial resistance R_{inter} can be represented as shown in Eq. (2) in relation to the contact length, where $\alpha(=\rho_{\mathrm{inter}}{}^{l}/C)$ is assumed to be constant. For sufficiently small contact length, R_{inter} becomes the dominant term, causing R_{total} to become roughly inversely proportional to the contact length.

Figure 3(a) presents the measured electrical resistance values plotted as functions of the inverse of contact length. The purple circles, green triangles and red crosses correspond to the data series as in Fig. 2, and corresponding TEM images are shown in Fig. 3(b), Fig. 1(d)–(f), and Fig. 3(c), respectively. Orange plots labelled as “15nm_2” are the data measured on the same specimen as the red cross plots but with the contact made on the opposite side of each MWCNTs [Fig. 3(d)]. These two data series, represented by the red and orange crosses, were taken from the same MWCNTs pair and show almost the same resistance, indicating the good reproducibility of this experiment and negligible effects of the electron irradiation during the measurements. However, it should be noted that the values are not exactly the same, probably because the results are sensitive to the geometry of the contact. The tip shapes and the distribution of Sn particles changed from Fig. 3(c) to 3(d) due to the sublimation of carbon atoms via Joule heating. Here, the resistance of the specimens of diameter 15 nm show an almost linear behaviour with respect to the inverse of contact length, at least for contact lengths smaller than ~50 nm; this findings is reasonable given Eq. (2). These curves’ slopes [i.e., α in Eq. (2)] are 990, 270, and 45 kΩ nm for the green triangles, red crosses and orange crosses, respectively. Here, we assume that $l = 0.51$ nm and $C = 3.2$ nm for MWCNTs of diameter 15 nm (see Supplementary Information). The electrical conductivity of the interface between MWCNTs is then estimated to be 2×10^2–4×10^3 S/m. The validity of this analysis can be verified by a comparison with the electrical conductivity of graphite along its *c*-axis. The *c*-axis conductivity of single-crystal graphite is typically on the order of 10^4 S/m (summarized in Ref. [22]), which is one or two orders of magnitude higher than that estimated in this study. However, in the case of the pyrolytic graphite, the typical conductivity of graphite is strongly impeded and reaches only ~10^2 S/m [22]. The basal plane of pyrolytic graphite has a good mosaic spread value, but orientation is not well spread with respect to the other axes. Therefore, pyrolytic graphite includes numerous stacking faults (i.e., not close-packed stacking) and has an elevated *c*-axis lattice parameter [23] compared to single-crystal graphite. Returning to our experiment, the situation is similar to that of pyrolytic graphite because the contact between two MWCNTs does not necessarily correspond to close-packed stacking. This lattice mismatch may be the reason for the depressed and variable (among specimens) electrical conductivity compared to that of single-crystal graphite. One would expect the outer diameter to have an effect on the interfacial resistance, however, no significant relationship was detected. This may be because the lattice mismatch is rather important for the interfacial transport than the diameter. Fuhrer *et al*. reported the formation of Schottky barriers between metallic and

semiconducting nanotubes, resulting in a low junction conductance two orders of magnitude smaller than that for metallic–metallic and semiconducting–semiconducting junctions [15]. However, this effect may be negligible in the present case, given the linear and symmetric I–V curves observed in this study [Fig. 1(g)]. This negligibility is possibly due to shared chiral indices between the two paired MWCNTs, given that they are both parts of a single original MWCNT. In addition, the negligibility may be due to the present study's high temperature (namely, room temperature) and/or larger nanotube diameter, thus producing a smaller band gap and Schottky barrier. In contrast, the resistance for the pair of MWCNTs of diameter 8 nm was not proportional to the inverse of the contact length. This result can be attributed to R_{CNT} because the contact length is large in the measurement region and R_{CNT} is high due to the small diameter. With increasing contact length, R_{inter} rapidly decreases, causing R_{CNT} to become dominant in the contact length effect. For sufficiently large contact lengths (i.e., for sufficiently small R_{inter} values), R_{CNT} is related to contact length as follows:

$$R_{\mathrm{CNT}} \approx \rho_{\mathrm{CNT}}\frac{L_1 - x}{S} + \rho_{\mathrm{CNT}}\frac{L_2 - x}{S} + \rho_{\mathrm{CNT}}\frac{x}{2S} = R_0' - \beta x. \#(3)$$

Here, ρ_{CNT} is the electrical resistivity of the MWCNT, while L_1, L_2 and S are the lengths and cross-sectional area of two MWCNTs, respectively. Therefore, R_{total} is proportional to the contact length for sufficiently high contact lengths with the slope: $\beta(=3\rho_{\mathrm{CNT}}/2S)$. We note that the electrical resistivity along radial direction of MWCNT is not considered in this model. This approximation can be justified by the experimental results of the electrical resistance measurements while changing the cross-sectional area of an identical MWCNT [24]. The electrical resistance of the MWCNT was inversely proportional to the cross-sectional area of MWCNT, indicating that the MWCNT can be considered as a normal cylinder. Here, we approximate the total resistance as

$$R_{\mathrm{total}} \approx \frac{\alpha}{x} - \beta x + R_0'', \#(4)$$

where $R_0'' = R_0 + R_0'$ is the contact-length independent resistance (see Supplementary Information as for the approximation validity). For $x = \sqrt{\alpha/\beta}$, the differentials of the interface- and bulk-dominant terms become equal. Assuming $\rho_{\mathrm{CNT}} \approx 10^{-6}\ \Omega\mathrm{m}$ [9,10], $\sqrt{\alpha/\beta}$ becomes 100–300 nm, though it depends on the cross-sectional area of MWCNTs. For contact lengths above 100–300 nm, the resistance behaviour becomes linear with respect to changes in contact length, and we can derive the resistivity of MWCNTs from the slope.

Figure 4(a) presents the results of electrical resistance measurements for a range of contact lengths above 150 nm. The plots labelled "8 nm" and "18 nm" show data for outertube–outertube contact as explained above. "8 nm" presents data using the same symbols as Fig. 2 and Fig. 3(a). A similar experiment in a telescoped nanotube (see Fig. 4(b), Supplementary Information, and Ref. [25]) was conducted because the resistance behaviour with respect to contact length could be same as that of the outertube–outertube slide. The "20–24 nm" data series name gives the outer diameters of the two coaxial MWCNTs forming the telescopic configuration. The resistance is almost linear with respect to contact length in Fig. 4(a). This behaviour is consistent with Eq. (4) and implies non-ballistic electron transport in MWCNTs. Assuming that the cross-sectional area of MWCNTs is $\pi(d_{\mathrm{out}}^2 - d_{\mathrm{in}}^2)/4$, where d_{out} and d_{in} are the MWCNTs outer and inner diameters, the electrical conductivities are estimated to be 2×10^5 S/m for MWCNTs of diameter 8 nm, 4×10^5 S/m for MWCNTs of diameter 18 nm, and 3×10^5 S/m for the telescoped MWCNT. The conductivities derived from the experiments are consistent with previous reports [9,10], confirming the validity of the present analysis and model. It is worth noting that the specimen showed negative Seebeck coefficient [24], indicating the carrier is electron, whereas it has reported that the pristine CNTs show positive values [5]. This can be due to the annealing effect when the specimen was cut off by self-Joule heating. According to the previous study [26], vacuum annealing changes the p-type CNT into n-type due to the desorption of the oxygen. The negative Seebeck coefficient suggests that the MWCNTs in the present study were dedoped and freed from the surface adsorption of molecules. In the case of the telescoped MWCNTs, the resistance behaviour becomes nonlinear around 200 nm, resulting in a large α value of ~6000 kΩ nm, even though its contact should be wider and stabler than an outertube–outertube contact. Given that similar behaviour was reported in Ref. [27], MWCNTs might in fact have a considerably higher resistance in the radial direction. However, we note that the experiments in Ref. [27] were probably not effectively at room temperature given the large electric current. We verified that at electric currents of ~50 μA, Sn particles melted, indicating an MWCNT temperature above 200°C.

In our model, the effect of the interface between MWCNTs becomes negligible for contact lengths sufficiently longer than $\sqrt{\alpha/\beta}$, which is a few hundred nanometers as estimated herein. Experimentally, the electrical resistance before and after cutting by Joule heating was compared (see Supplementary Information), and it increased from 15 kΩ to 18 kΩ by the presence of the interface, supporting that the interfacial resistance can be non-dominant. As for graphite, the electrical conductivity of pyrolytic graphite along the *c*-axis is typically two orders of magnitude smaller than that of single-crystal graphite, whereas the in-plane conductivity of pyrolytic graphite is of comparable magnitude to that of single-crystal graphite [22]. This disparity may be due to sufficiently large contact areas between graphene layers. These results suggest that macroscopic MWCNT assemblies such as ropes and films can show electrical conductivities comparable to those of individual MWCNTs if each contact is sufficiently long (in concrete terms, more than a few hundred nanometers).

Conclusions

In summary, we used TEM measurements of electrical resistance over a range of contact lengths to obtain experimental values for two main electrical transport factors in the assembly of MWCNTs: the CNT and interface electrical conductivities. The interfacial conductivity is on the order of 10^2–10^3 S/m, and the CNT conductivity is on the order of 10^5 S/m. These findings suggest that the effect of the interface becomes negligible at contact lengths longer than a few hundred nanometers. This study has fundamental implications for the physics of CNT-based electronics and their applications.

Author Contributions

All authors contributed to the discussion, interpretation, and writing the manuscript of this study. H.H. performed all experiments and analyses in the main text. S.N. partially contributed to the TEM observation. K.H. supervised the study.

Conflicts of interest

There are no conflicts to declare.

Acknowledgements

This work was supported by JST CREST Grant Number JPMJCR17I5, Japan.

References

1 P. Jarosz, C. Schauerman, J. Alvarenga, B. Moses, T. Mastrangelo, R. Raffaelle, R. Ridgley, B. Landi, *Nanoscale*, 2011, **3**, 4542.
2 P. R. Jarosz, A. Shaukat, C. M. Schauerman, C. D. Cress, P. E. Kladitis, R. D. Ridgley, and B. J. Landi, *ACS Appl. Mater. Interfaces*, 2012, **4**, 1103.
3 F. Valentini, S. Orlanducci, M. L. Terranova, A. Amine, and G. Palleschi, *Sens. Actuators B*, 2004, **100**, 117.
4 B. L. Allen, P. D. Kichambare, and A. Star, *Adv. Mater*., 2007, **19**, 1439.
5 Y. Nakai, K. Honda, K. Yanagi, H. Kataura, T. Kato, T. Yamamoto, and Y. Maniwa, *Appl. Phys. Express*, 2014, **7**, 025103.
6 Y. Ichinose, A. Yoshida, K. Horiuchi, K. Fukuhara, N. Komatsu, W. Gao, Y. Yomogida, M. Matsubara, T. Yamamoto, J. Kono, and K. Yanagi, *Nano Lett*., 2019, **19**, 7370.
7 P. Kim, L. Shi, A. Majumdar, and P. L. McEuen, *Phys. Rev. Lett.,* 2001, **87**, 215502.
8 M. Fujii, X. Zhang, H. Ago, K. Takahashi, T. Ikuta, H. Abe, and T. Shimazu, *Phys. Rev. Lett.,* 2005, **95**, 065502.
9 T. W. Ebbesen, H. J. Lezec, H. Hiura, J. W. Bennett, H. F. Ghaemi, and T. Thio, *Nature,* 1996, **382**, 54.
10 T. D. Yuzvinsky, W. Mickelson, S. Aloni, S. L. Konsek, A. M. Fennimore, G. E. Begtrup, A. Kis, B. C. Regan, and A. Zettle, *Appl. Phys. Lett.,* 2005, **87**, 083103.
11 Y. Inoue, Y. Suzuki, Y. Minami, J. Muramatsu, Y. Shimamura, K. Suzuki, A. Ghemes, M. Okada, S. Sakakibara, H. Mimura, and K. Naito, *Carbon,* 2011, **49**, 2437.
12 L. Shi, D. Li, C. Yu, W. Jang, D. Kim, Z. Yao, P. Kim, and A. Majumdar, *J. Heat Transfer*., 2003, **125(5)**, 881.
13 H. Hamasaki, S. Takimoto, and K. Hirahara, *Nano Lett.*, 2021, **21**, 3134.
14 J. Yang, S. Waltermire, Y. Chen, A. A. Zinn, T. T. Xu, and D. Li, *Appl. Phys. Lett*., 2010, **96**, 023109.
15 M. S. Fuhrer, J. Nygard, L. Shih, M. Forero, Y. G. Yoon, M. C. S. Mazzoni, H. J. Choi, J. Ihm, S. G. Louie, A. Zettl, and P. L. McEuen, *Science*, 2000, **288**, 494.
16 P. N. Nirmalraj, P. E. Lyons, S. De, J. N. Coleman, and J. J. Boland, *Nano lett.*, 2009, **9**, 3890.
17 C. J. Barnett, C. Evans, J. E. McCormack, C. E. Gowenlock, P. Dunstan, W. Adams, A. O. White, and A. R. Barron, *Nano Lett.*, 2019, **19**, 4861.
18 F. Xu and Y. Zhu, *Adv. Mater*., 2012, **24**, 5117.
19 S. Ye, A. R. Rathmell, Z. Chen, I. E. Stewart, and B. J. Wiley, *Adv. Mater*., 2014, **26**, 6670.
20 X.-B. Xu, Z.-M. Li, L. Shi, X.-C. Bian, and Z.-D. Xiang, *Small*, 2007, **3**, 408.
21 S. Gao, X. Zhao, Q. Fu, T. Zhang, J. Zhu, F. Hou, J. Ni, C. Zhu, T. Li, Y. Wang, V. Murugadoss, G. A. M. Mersal, M. M. Ibrahim, Z. M. El-Bahy, M. Huang, and Z. Guo, *J. Mater. Sci. Technol*., 2022, **126**, 152.
22 D. Z. Tsang, and M. S. Dresselhaus, *Carbon*, 1976, **14**, 43.
23 K. Kusakabe, A. Wake, A. Nagakubo, K. Murashima, M. Murakami, K. Adachi, and H. Ogi, *Phys. Rev. Materials*, 2020, **4**, 043603.
24 H. Hamasaki et al., *In preparation*.
25 J. Cumings, and A. Zettle, *Science*, 2000, **289**, 602.
26 V. Derycke, R. Martel, J. Appenzeller, and Ph. Avouris, *Nano Lett.*, 2001, **1**, 453.
27 J. Cumings, and A. Zettle, *Phys. Rev. Lett*., 2004, **93**, 086801.

COMMUNICATION

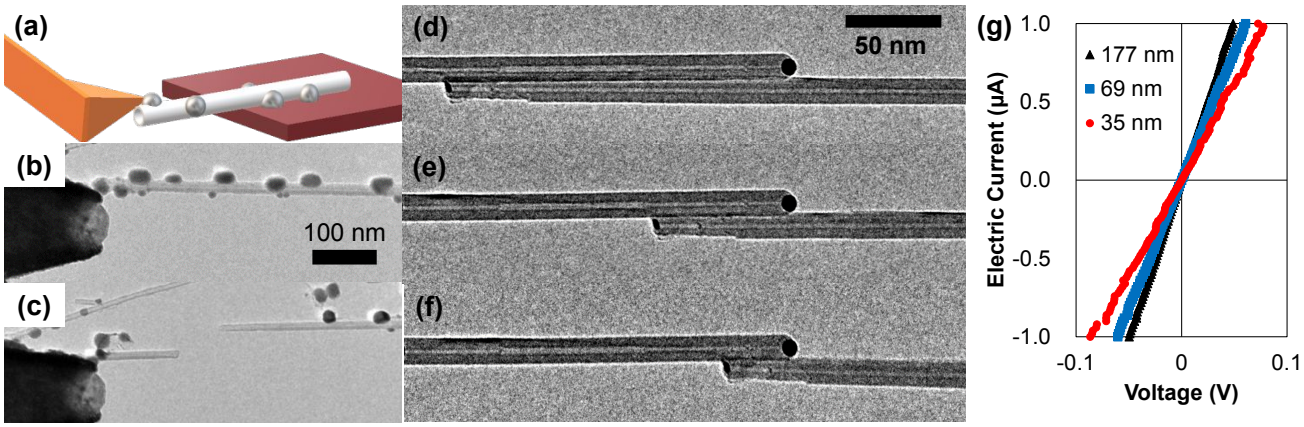

Figure 1. *In situ* measurement of electrical resistance of parallel contact between two multiwalled carbon nanotubes (MWCNTs) with varying the contact length. (a) Schematic and (b) actual transmission electron microscopy (TEM) image of the experimental setup. (c) TEM image after MWCNT cutoff via self-Joule heating. After cutting, one MWCNT is brought into contact with the other. (d, e, f) TEM images of outertube–outertube contacts of various contact lengths. (g) Current–voltage relationships for (d) (black), (e) (blue), and (f) (red). The legend presents contact length.

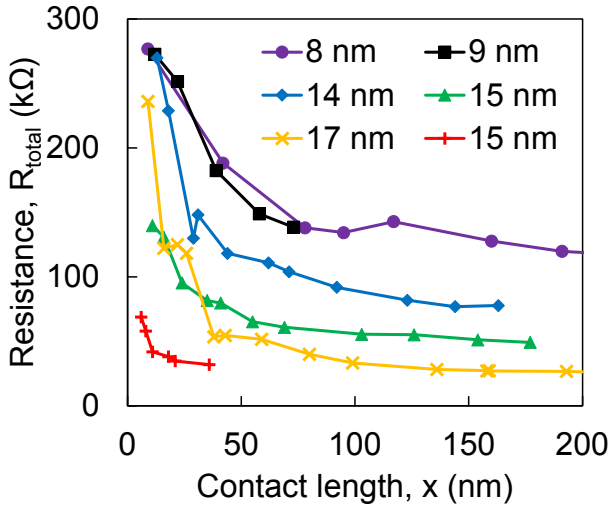

Figure 2. Electrical resistance of single contact between multiwalled carbon nanotubes as a function of contact length. Legend indicates the outer diameter of each multiwalled carbon nanotube.

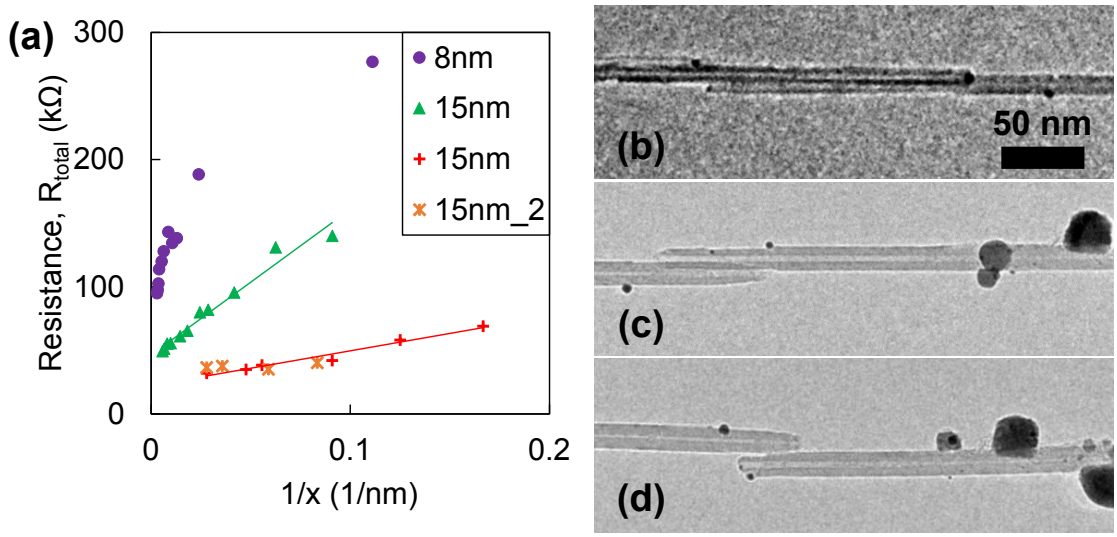

Figures 3. Electrical resistance of single contact between multiwalled carbon nanotubes (MWCNTs) as a function of the inverse of contact length. (a) Purple circles, green triangles, and red crosses represent the data shown in Fig. 2 using the same symbols. Orange crosses represent the data for the same pair of MWCNTs as red crosses but with the contact on the opposite side of each MWCNT. (b)–(d) Transmission electron microscopy (TEM) images corresponding to (b) purple circles, (c) red crosses, and (d) orange crosses. TEM images corresponding to green triangles are shown in Fig. 1(d)–(f). The shapes of the MWCNT tips changed between (c) and (d) because of MWCNT sublimation.

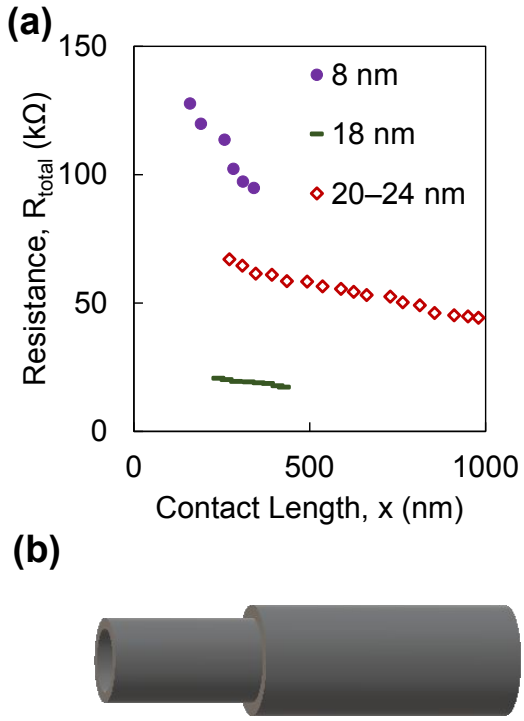

Figure 4. Electrical resistance of single contact between multiwalled carbon nanotubes (MWCNTs) as a function of contact length for contact lengths over 150 nm. (a) Purple circles and black bars represent outertube–outertube contact data; the legend indicates the outer diameter of each MWCNTs. The brown diamonds represent telescoped MWCNT data; in this case, the legend indicates the outer diameter of the core and the housing MWCNTs. (b) Schematic of telescoped MWCNT.